Journal of Nuclear Medicine, published on June 18, 2015 as doi:10.2967/jnumed.114.153346

WORD COUNT 4583

INTRA-ARTERIAL HEPATIC SPECT/CT IMAGING USING TECHNETIUM-99M MACRO-AGGREGATED ALBUMIN IN PREPARATION FOR RADIOEMBOLIZATION

Vanessa L Gates[1], Nimarta Singh[2], Robert J Lewandowski[2], Stewart Spies[1], Riad Salem[2]

[1]Department of Radiology, Section of Interventional Radiology, Northwestern Memorial Hospital, Robert H. Lurie Comprehensive Cancer Center, Chicago IL

[2]Department of Medicine, Division of Hematology and Oncology, Robert H. Lurie Comprehensive Cancer Center, Northwestern University, Chicago, IL

Corresponding Author: Riad Salem, MD, MBA

Director, Interventional Oncology

Section of Interventional Radiology

Department of Radiology

676 N. St. Clair, Suite 800

Chicago, Illinois 60611 USA

email:r-salem@northwestern.edu

Role of Funding: There was no funding provided for this study.

Conflict of Interest: RJL and RS are advisors to BTG. None of the other authors have any conflict of interest.

ABSTRACT

Current standard practice for radioembolization (RE) treatment planning makes use of nuclear medicine imaging (NMI) of technicium-99m macro-aggregated albumin (MAA) arterial distributions for the assessment of lung shunting and extra-hepatic uptake. Our aim was to retrospectively compare NMI with that of mapping angiography in the detection and localization of extra-hepatic MAA and to evaluate the typical and atypical findings of NMI in association of catheter placement.

Methods: 174 patients underwent diagnostic angiography in preparation for radioembolization. MAA was administered to the liver via a microcatheter positioned in the desired hepatic artery. Planar scintigraphy imaging followed by SPECT/CT imaging was obtained within 2 hours. All images were reviewed for hepatic and extra-hepatic MAA deposition and compared to the mapping angiogram.

Results: Intrahepatic lobe shunting on was present on NMI in only 2.9% of the cases but was present in 62.5% of the patients with PVT. Extra-hepatic distributions included lungs (100%), the gallbladder (49%) if present, and locations involving hepaticoenteric arterial anatomy recognized on angiograms (16%). Free pertechnetate was identified on 38% of the NMI. 3% of NMI showed alternative findings such as a thyroid nodule or metallic artifact.

Conclusions: Patients who are being considered for RE should undergo both angiographic and scintigraphic for assessment of hepaticoenteric arterial anatomy, hepatopulmonary shunting, and appropriate dosimetry considerations. Knowledge of the expected distribution of MAA with normal variants and potential non-target delivery to adjacent structures is critical in improving clinical outcomes.

Key Words: liver neoplasms, radiotherapy, radioembolization, technetium-99m macro-aggregated albumin, SPECT/CT, Yttrium-90 microspheres

Currently, nuclear medicine imaging (NMI) of technecium-99m labeled macro-aggregated albumin (^{99m}Tc-MAA) is performed routinely prior to radioembolization (RE) for the assessment of lung shunting and extra-hepatic uptake. This is widely recognized to be important for minimizing the risk of potentially debilitating adverse events such as radiation induced pneumonitis or radiation gastritis/duodenitis after RE using ^{90}Y microspheres for inoperable hepatic tumors (*1, 2*). The seminal work in a canine liver model demonstrating the safety and feasibility of using ^{90}Y microsphere therapy for hepatic malignancies was reported in the late 1980's. Human studies of ^{90}Y microsphere therapy in liver applications followed from the late 1980's through the 1990's. These investigations established the safety of ^{90}Y for intrahepatic applications and the optimal dosimetry for tumor radiation kill, while minimizing exposure to normal liver tissue (*3-8*).

Given the similarities in sizes of ^{90}Y microspheres (20-40 microns) and ^{99m}Tc-MAA (20-50 microns), the pattern of ^{99m}Tc-MAA deposition as determined from a high resolution SPECT/CT acquisition serves as a surrogate to demonstrate how ^{90}Y microspheres will localize during treatment. Radioembolization has evolved for the palliative treatment of patients with primary and secondary malignancies. Meticulous pre-treatment planning with angiography and ^{99m}Tc-MAA scintigraphy allows for low toxicity profile, increased response rates, and low incidence of post-treatment complications for patients (*9*). The purpose of this paper is to demonstrate the typical and atypical findings of ^{99m}Tc-MAA distribution obtained as part of pre-therapeutic planning for RE with ^{90}Y microspheres.

MATERIALS AND METHODS

Patients

This research was completed with the approval of the Northwestern University Investigational Review Board, all subjects signed a written informed consent, and procedures followed were in accordance with the ethical standards of the Helsinki Declaration of 1975, as revised in 2008. Between March, 2009 and September, 2010, 174 patients underwent pretreatment diagnostic angiography with ^{99m}Tc-MAA administered via a microcatheter positioned in a hepatic artery (placed at the discretion of the attending interventional radiologist). Subsequently, all were treated with ^{90}Y glass microspheres (TheraSphere®, BTG International). Technical details for radioembolization have been discussed in detail elsewhere **(*10, 11*).** Ninety-two patients were being treated for metastatic disease of the liver (colorectal cancer (40), neuroendocrine disease (20), cholangiocarcinoma (15), and miscellaneous origin (16). Eighty-three patients were being treated for primary HCC.

Diagnostic Arterial Imaging

As part of the routine diagnostic work-up completed 1 to 2 weeks prior to radioembolization treatment, all patients were administered 74 MBq to 148 MBq of ^{99m}Tc-MAA via a microcatheter positioned in an hepatic artery. Static scintigraphy imaging followed by SPECT/CT imaging was initiated within 2 hours following the administration of ^{99m}Tc-MAA. For planar imaging, the patient was positioned supine under the gamma camera and 4 images were acquired: anterior and posterior images of the abdomen and anterior and posterior images of the thorax. Each image was acquired for 5 minutes in a 256X256 matrix without scatter correction. Region of interest to determine counts was drawn around the liver activity, each individual lung activity, a background region below the liver, and background regions on the lateral side of each lung. The cardiac pool was not included in the lung count estimates. The liver to lung shunt was calculated as the geometric mean of the net counts within the lungs divided by the sum of the geometric mean of the net liver counts and the net lungs counts.

Arterial distribution of the particles was quantified from SPECT/CT fused images that were obtained on the Siemens Symbia T2 (SPECT/CT) using an energy window of 140 ± 10.5 keV and 128 X128 acquisition matrix with 60 frames (angular step 3 degrees) at a rate of 35 seconds per frame. Attenuation correction was achieved through the CT acquisition (130 kV, 25 mAs, B30 kernel, and 5 mm slices). Reconstruction of the images was achieved using FLASH 3D without scatter correction, which is a proprietor iterative method of ordered subset expectation maximization using 5 iterations and 8 subsets. Reconstructed images were fused and analyzed with Syngo TrueD (Siemens AG, 2008).

Image Interpretation and Categorization

The reference standard for hepaticoenteric arterial anatomy was the mapping angiogram and associated report that was generated by 6 experienced interventional radiologists. All scintigraphic images were reviewed for hepatic and extra-hepatic ^{99m}Tc-MAA deposition by 3 experienced nuclear medicine physicians using a Syngo workstation (VE25A; Siemens Healthcare). Images were read in the following order: planar, SPECT, and SPECT/CT.

For this review of ^{99m}Tc-MAA distribution following hepatic arterial administration, cases were divided into three categories as hepatic distributions, extra-hepatic distributions, and normal distribution variants (defined as findings expected due to delabeled ^{99m}Tc-MAA). Results from nuclear medicine imaging were also compared to expected distributions from the mapping angiograms. Statistical comparisons and significances were achieved through the Student’s Paired t-Test.

RESULTS

Patient Sample and Diagnostic Arterial Imaging

All patients successfully underwent planning angiography with the administration of 131 ± 38 MBq (ranging from 63 MBq to 178 MBq) ^{99m}Tc-MAA and, within 2 hours, underwent successful planar imaging of the thorax and abdomen followed by SPECT/CT imaging. There were no reportable or recordable medical events.

Category 1: Hepatic Distributions

Distribution of ^{99m}Tc-MAA within the liver depends on the microcatheter placement within the hepatic artery and the arterial supply to the tumor and normal hepatic tissue. Three major patterns of tumor perfusion are observed with ^{99m}Tc-MAA SPECT/CT images: (1) increased uptake of ^{99m}Tc-MAA in the center of tumor, (2) decreased central radiotracer uptake within the tumor, and (3) mixed/diffuse radiotracer uptake within the liver (Supplemental Figures 1-3).

The distribution of catheter placement included 1 whole liver, 158 lobar, and 15 segmental. The majority of ^{99m}Tc-MAA administrations were with the microcatheter within the right or left hepatic artery, supplying 1 lobe of the liver. The right lobe or a segment within the right lobe was found to be perfused in 128 cases. Of the 128 right hepatic artery administrations, a subset of 51 cases involving the microcatheter positioned proximal to the right hepatic artery branch was examined for caudate lobe distributions. Within this subset, 19 cases (37%) demonstrated activity within the caudate lobe. This was consistent with the known position of the microcatheter to the caudate artery (Supplemental Figure 3).

Of the 174 cases, 15 cases involved administration of ^{99m}Tc-MAA through a microcatheter placed in a segmental branch off either the right or left hepatic artery. For the purpose of this study, placement through a separate middle hepatic artery was considered to be a segmental administration (Supplemental Figure 4).

Portal vein thrombosis (PVT) is thought to contribute to some of the cases involving lobe to lobe shunting. However, of the 8 patients with PVT, intrahepatic communications were only demonstrated on 5 (all HCC) NMI and 4 on the mapping angiogram (Figure 1).

Twenty-two of the 174 cases involved SPECT/CT imaging of patients who had received previous hepatic treatments including radiofrequency ablation (RFA), transarterial chemoembolization (TACE), RE, or hepatic resections.

Category 2: Extra-hepatic Distributions

All cases showed some level of deposition of ^{99m}Tc-MAA to the lungs. The mean percentage of activity shunted from the liver to the lungs was 7.71 ± 7.74 % (range: 0.70% to 57.40%). For the patients with HCC, the mean percentage of activity shunted from the liver to the lungs was 9.37 ± 9.62 % (range: 0.80% to 57.40%). For the patients with primary disease metastatic to the liver, the mean percentage of activity shunted from the liver to the lungs was 6.20 ± 5.13 % (range: 0.70% to 30.70%). For one case, ^{99m}Tc-MAA began to significantly break down into free technetium and varied sized particles within 75 minutes following the administration of ^{99m}Tc-MAA. Due to this accelerated breakdown of the radiopharmaceutical, the pulmonary shunt calculation may be artificially elevated. The concentration of the breakdown of the radiopharmaceutical is best illustrated as the image intensity within the bladder exceeding that within the lungs.

Twenty-one of the 174 cases reviewed had hepaticoenteric arterial communications. Eight of these cases involved the purposeful placement of the microcatheter into an artery supplying extra-hepatic tissue (1 falciform artery, 2 gastroduodenal arteries (GDA), and 5 gastric arteries (GA)). **D**uodenal uptake was from ^{99m}Tc-MAA administration through a catheter placed in the right hepatic artery but proximal to the GDA (Figure 2). ^{99m}Tc-MAA uptake within the anterior abdominal wall was due to ^{99m}Tc-MAA administration through both a microcatheter placed within the middle hepatic artery with the falciform artery arising off the middle hepatic artery (Figure 3). Focal activity

corresponding to the medial left lobe hepatoma and focal activity within the medial wall of the proximal stomach was due to a replaced left gastric artery (Figure 4).

For treatment, distribution to the gallbladder can often be avoided by placing the microcatheter distal to the cystic artery. However, there are cases in which the gallbladder will receive a radiation dose because the microcatheter can only be placed proximal to the cystic artery. Reviewing the images in a subset of 51 cases involving patients with gallbladders still present showed 25 cases involving ^{99m}Tc-MAA distribution to the gallbladder wall. Treatment was still performed on patients when the microcatheter could be placed distally as well as on patients in which the microcatheter required proximal placement.

Category 3: Normal Distribution Variants

In vivo formation of free pertechnetate was considered part of the standard distribution when the ^{99m}Tc-MAA imaging demonstrated activity within the lumen of the stomach along with activity in either the thyroid or salivary glands or both (**Figure 5**). Fragmented ^{99m}Tc-MAA was also considered a normal distribution variant when the imaging indicated activity within the kidneys as well as the lumen of the stomach. In reviewing all 174 ^{99m}Tc-MAA image case reports, we found that 66 of the 174 cases showed indication of free pertechnetate or fragmented ^{99m}Tc-MAA.

Alternative findings included both radioactive distributions that were not related to arterial distribution of ^{99m}Tc-MAA as well as anatomical notations based on the low dose CT image used for attenuation correction. Two examples included ^{99m}Tc pertechnetate distribution to the thyroid, in which imaging showed hyperactivity within the thyroid nodule (**Figure 5**) and focal uptake of ^{99m}Tc-labelled fragmented MAA or ^{99m}Tc pertechnetate within the renal poles that was different from the homogenous distribution observed within the kidneys related to physiological breakdown of ^{99m}Tc-MAA. Gallstones within the gallbladder will sometimes create a density artifact on the attenuation correction map. As a result of the density artifact, a focal area of the

gallbladder wall may appear to receive a higher concentration of ^{99m}Tc-MAA activity, but this is artifactual. Five of the 174 cases reviewed showed alternative findings.

DISCUSSION

Radioembolization has evolved for the palliative treatment of patients with primary and secondary malignancies. The safety of this therapy requires detailed planning angiography with MAA administration. A detailed discussion of considerations of normal hepatic perfusion and hepaticoenteric arterial anatomy in context of radioembolization has been published elsewhere (*10, 12-16*). This study reports our experience in treatment planning for 174 patients. We review the imaging findings following intra-hepatic MAA administration and report the incidence of normal variants and extra-hepatic deposition from both NMI and planning angiography (Figure 1).

Regardless of location within the liver, greater uptake of ^{99m}Tc-MAA is expected in regions of the tumor given that tumor beds are predominantly supplied via the arterial system of the liver whereas normal hepatic parenchyma is supplied by the portal system. Three major patterns of tumor perfusion are observed with ^{99m}Tc-MAA SPECT/CT images (Supplemental Figures 1-3). A detailed discussion of considerations of normal hepatic perfusion and hepaticoenteric arterial anatomy in context of radioembolization has been published elsewhere (*10, 12-16*). In a recent publication by Ilhan et al., SPECT/CT images were reviewed for tumor uptake distribution and graded based on concentration of MAA as well as distribution within the tumor (*17*). The majority of lesions were of grade 1 (high uptake, homogeneous distribution) or grade 2 (high uptake, heterogeneous distribution) (Supplemental Figures 1-2). Patient with Grade 1 or 2 also demonstrated better tumor response. Along these lines, several authors propose a more quantitative method using MAA SPECT/CT to determine a threshold dose for treatment with Y-90 microspheres (*14, 18-20*).

Several authors are using MAA SPECT/CT to determine a threshold dose for treatment with Y-90 microspheres. For glass microspheres. Garin et al. reported that a tumor dose exceeding 205 Gy and Chiesa et al. reported that a tumor dose of 257 Gy were required to induce tumor response (*21, 22*). Similarly, Riaz et al. reported that using segmental

dosimetry (segment receives 100% of radiation dose) that a dose greater than 190 Gy was required to perform a segmentectomy (Supplemental Figure 4) (*23*).

For patients being treated for HCC with portal vein thrombosis (PVT), the SPECT/CT does play an important role for doing more tumor based treatment planning dosimetry. In these patients, PET/CT demonstrated that microspheres distributed within the PVT (*24*). Overall survival of these patients improved using the “boosted” personalized dose method described by Garin et al. in which the tumor dose of 205 Gy was achieved through increasing the lobar dose to 150 Gy maximum (*25*). From our study, the perfused volume would include both the right and left lobar volumes for 62.5% of the patients with HCC and PVT. Therefore, a little less than half this population would be under dosed using the standard lobar dose of 120 Gy.

Another potential concern for performing personalized dosimetry based on SPECT/CT may be gallbladder uptake of microspheres that would result in radiation-induced cholecystitis. Our study showed that for patients with a gallbladder present the MAA would be taken up by 49% of the patients when the microcatheter is placed proximally to the cystic artery. However, by adjusting the position of the microcatheter, the percent of patients with gallbladder uptake could be reduced to 16%. This is similar to a published SPECT/CT study, in which the repositioning of the microcatheter resulted in a reduction of gallbladder visibility in 90% of the cases (*26*).

The question still remains as to whether we need to take actions like coiling the cystic artery or surgically removing the gall bladder to prevent radiation induced cholecystitis. In a study performed at our institution, we only saw 2 cases (0.6%) of radiation-induced cholecystitis, which is similar to other published results (*27, 28*). None of the patients in this study developed cholecystitis despite showing MAA uptake within the gallbladder.

If AV shunting into branches of the hepatic vein is present, then ^{90}Y microsphere can reach the pulmonary circulation, producing unwanted pulmonary toxicity. NMI from this study showed ^{99m}Tc-MAA distribution to the lungs from all of the patients. One possible

reason for this discrepancy is that the package insert indicates that up to 1% to 2% of these particles may be less than 15 microns. The smaller particle diameter (< 8 microns) facilitates movement into the lungs through normal vasculature rather than through malignant AV communications, consequently leading to greater activity detected within the lungs. Another possible reason could be due to the timing between the MAA production, the MAA infusion, and the NMI. The useful life of the particles is approximately 6 hours. As a result, longer delays could result in artificially elevated lung shunt values (*29*).

AV shunting is well known to exist in HCC (*30*). It has also been suggested that higher percentages of lung shunting are seen with HCC than with metastatic disease to the liver (*30*). Although the range of percentages of lung shunting are comparable between patients with HCC and patients with metastatic disease to the liver, the mean values from this cohort are statistically different (p=0.004).

Focal increase in ^{99m}Tc-MAA activity within the falciform artery, phrenic artery, duodenum, gastric lumen or anywhere along the gastrointestinal tract is concerning for extra-hepatic shunting due to hepaticoenteric arterial communications (*15*). These vessels include the falciform, accessory or left phrenic, right or accessory gastric arteries (from the left hepatic artery), supraduodenal, retroduodenal, and accessory right hepatic artery feeding segment 6 (from gastroduodenal artery). Using the angiogram technique outlined in Lewandowski et al., none of our ^{99m}Tc-MAA SPECT/CT images showed extra-hepatic uptake due to hepaticoenteric arterial communications that was not also observed in the planning angiogram or flat-panel CBCT (*10, 12*). To illustrate the uptake of ^{99m}Tc-MAA due to these arterial distribution, eight patients were purposefully administered the radiopharmaceutical proximal to the uncoiled vessel. Prior to treatment with microspheres, the vessel was either coiled or the microcatheter was placed distally.

When comparing CBCT versus MAA scintigraphy, Louie et al. showed that CBCT demonstrated 19% extra-hepatic enhancement that were not evident on MAA

imaging.(*31*) Similarly, our study showed that with DSA and CBCT angiography can predict 99.5% of the hepatic and extra-hepatic distribution.

CONCLUSION

Patients being considered for RE should undergo angiographic and scintigraphic assessment with ^{99m}Tc-MAA using planar and tomography imaging for assessment of hepaticoenteric arterial communications, hepatopulmonary shunting, and appropriate dosimetry considerations. A thorough review of the NMI findings is essential to ensure proper catheter positioning in order to optimize treatment outcomes.

REFERENCES

1. Leung WT, Lau WY, Ho SK, et al. Measuring lung shunting in hepatocellular carcinoma with intrahepatic-arterial technetium-99m macroaggregated albumin. *J Nucl Med.* 1994;35:70-73.

2. Leung TW, Lau WY, Ho SK, et al. Radiation pneumonitis after selective internal radiation treatment with intraarterial 90yttrium-microspheres for inoperable hepatic tumors. *Int J Radiat Oncol Biol Phys.* 1995;33:919-924.

3. Andrews JC WS, Ackermann RJ, Cotton LA, Ensminger WD, Shapiro B. Hepatic radioembolization with yttrium-90 containing glass microspheres: preliminary results and clinical follow-up. *J Nucl Med.* 1994;35:1637-1644

4. Wollner I, Knutsen C, Smith P, et al. Effects of hepatic arterial yttrium 90 glass microspheres in dogs. *Cancer.* 1988;61:1336-1344.

5. Herba MJ, Illescas FF, Thirlwell MP, et al. Hepatic malignancies: improved treatment with intraarterial Y-90. *Radiology.* 1988;169:311-314.

6. Shepherd FA, Rotstein LE, Houle S, Yip TC, Paul K, Sniderman KW. A phase I dose escalation trial of yttrium-90 microspheres in the treatment of primary hepatocellular carcinoma. *Cancer.* 1992;70:2250-2254.

7. Houle S, Yip TK, Shepherd FA, et al. Hepatocellular carcinoma: pilot trial of treatment with Y-90 microspheres. *Radiology.* 1989;172:857-860.

8. Dancey JE, Shepherd FA, Paul K, et al. Treatment of nonresectable hepatocellular carcinoma with intrahepatic 90Y-microspheres. *J Nucl Med.* 2000;41:1673-1681.

9. Denecke T, Ruhl R, Hildebrandt B, et al. Planning transarterial radioembolization of colorectal liver metastases with Yttrium 90 microspheres: evaluation of a sequential diagnostic approach using radiologic and nuclear medicine imaging techniques. *Eur Radiol.* 2008;18:892-902.

10. Lewandowski RJ, Sato KT, Atassi B, et al. Radioembolization with 90Y microspheres: angiographic and technical considerations. *Cardiovasc Intervent Radiol.* 2007;30:571-592.

11. Salem R, Thurston KG. Radioembolization with 90Yttrium microspheres: a state-of-the-art brachytherapy treatment for primary and secondary liver malignancies. Part 1: Technical and methodologic considerations. *J Vasc Interv Radiol.* 2006;17:1251-1278.

12. Liu DM, Salem R, Bui JT, et al. Angiographic considerations in patients undergoing liver-directed therapy. *J Vasc Interv Radiol.* 2005;16:911-935.

13. Lenoir L, Edeline J, Rolland Y, et al. Usefulness and pitfalls of MAA SPECT/CT in identifying digestive extrahepatic uptake when planning liver radioembolization. *Eur J Nucl Med Mol Imaging.* 2012;39:872-880.

14. Ahmadzadehfar H, Duan H, Haug AR, Walrand S, Hoffmann M. The role of SPECT/CT in radioembolization of liver tumours. *Eur J Nucl Med Mol Imaging.* 2014;41 Suppl 1:S115-124.

15. Ahmadzadehfar H, Sabet A, Biermann K, et al. The significance of 99mTc-MAA SPECT/CT liver perfusion imaging in treatment planning for 90Y-microsphere selective internal radiation treatment. *J Nucl Med.* 2010;51:1206-1212.

16. Hamami ME, Poeppel TD, Muller S, et al. SPECT/CT with 99mTc-MAA in radioembolization with 90Y microspheres in patients with hepatocellular cancer. *J Nucl Med.* 2009;50:688-692.

17. Ilhan H, Goritschan A, Paprottka P, et al. Systematic Evaluation of Tumoral 99mTc-MAA Uptake Using SPECT and SPECT/CT in 502 Patients Before 90Y Radioembolization. *J Nucl Med.* 2015;56:333-338.

18. Chiesa C, Lambert B, Maccauro M, et al. Pretreatment Dosimetry in HCC Radioembolization with 90Y Glass Microspheres Cannot Be Invalidated with a Bare Visual Evaluation of 99mTc-MAA Uptake of Colorectal Metastases Treated with Resin Microspheres. *J Nucl Med.* 2014;55:1215-1216.

19. Chiesa C, Maccauro M, Romito R, et al. Need, feasibility and convenience of dosimetric treatment planning in liver selective internal radiation therapy with (90)Y microspheres: the experience of the National Tumor Institute of Milan. *Q J Nucl Med Mol Imaging.* 2011;55:168-197.

20. Garin E, Lenoir L, Rolland Y, et al. Dosimetry based on 99mTc-macroaggregated albumin SPECT/CT accurately predicts tumor response and survival in hepatocellular carcinoma patients treated with 90Y-loaded glass microspheres: preliminary results. *J Nucl Med.* 2012;53:255-263.

21. Garin E, Lenoir L, Edeline J, et al. Boosted selective internal radiation therapy with Y-loaded glass microspheres (B-SIRT) for hepatocellular carcinoma patients: a new personalized promising concept. *Eur J Nucl Med Mol Imaging.* 2013; 40:1057-1068.

22. Chiesa C, Mira M, Maccauro M, et al. A dosimetric treatment planning strategy in radioembolization of hepatocarcinoma with 90Y glass microspheres. *Q J Nucl Med Mol Imaging.* 2012;56:503-508.

23. Riaz A, Gates VL, Atassi B, et al. Radiation segmentectomy: a novel approach to increase safety and efficacy of radioembolization. *Int J Radiat Oncol Biol Phys.* 2011;79:163-171.

24. Padia SA, Alessio A, Kwan SW, Lewis DH, Vaidya S, Minoshima S. Comparison of positron emission tomography and bremsstrahlung imaging to detect particle distribution in patients undergoing yttrium-90 radioembolization for large hepatocellular carcinomas or associated portal vein thrombosis. *J Vasc Interv Radiol.* 2013;24:1147-1153.

25. Garin E, Rolland Y, Edeline J, et al. Personalized Dosimetry with Intensification Using 90Y-Loaded Glass Microsphere Radioembolization Induces Prolonged Overall Survival in Hepatocellular Carcinoma Patients with Portal Vein Thrombosis. *J Nucl Med.* 2015;56:339-346.

26. Prince JF, van den Hoven AF, van den Bosch MA, Elschot M, de Jong HW, Lam MG. Radiation-induced cholecystitis after hepatic radioembolization: do we need to take precautionary measures? *J Vasc Interv Radiol.* 2014;25:1717-1723.

27. Sag AA, Savin MA, Lal NR, Mehta RR. Yttrium-90 radioembolization of malignant tumors of the liver: gallbladder effects. *AJR Am J Roentgenol.* 2014;202:1130-1135.

28. Atassi B, Bangash AK, Lewandowski RJ, et al. Biliary sequelae following radioembolization with Yttrium-90 microspheres. *J Vasc Interv Radiol.* 2008;19:691-697.

29. De Gersem R, Maleux G, Vanbilloen H, et al. Influence of time delay on the estimated lung shunt fraction on 99mTc-labeled MAA scintigraphy for 90Y microsphere treatment planning. *Clin Nucl Med.* 2013;38:940-942.

30. Ho S, Lau WY, Leung WT, et al. Arteriovenous shunts in patients with hepatic tumors. *J Nucl Med.* 1997;38:1201-1205.

31. Louie JD, Kothary N, Kuo WT, et al. Incorporating Cone-beam CT into the Treatment Planning for Yttrium-90 Radioembolization. *J Vasc Interv Radiol.* 2009;20:606-613.

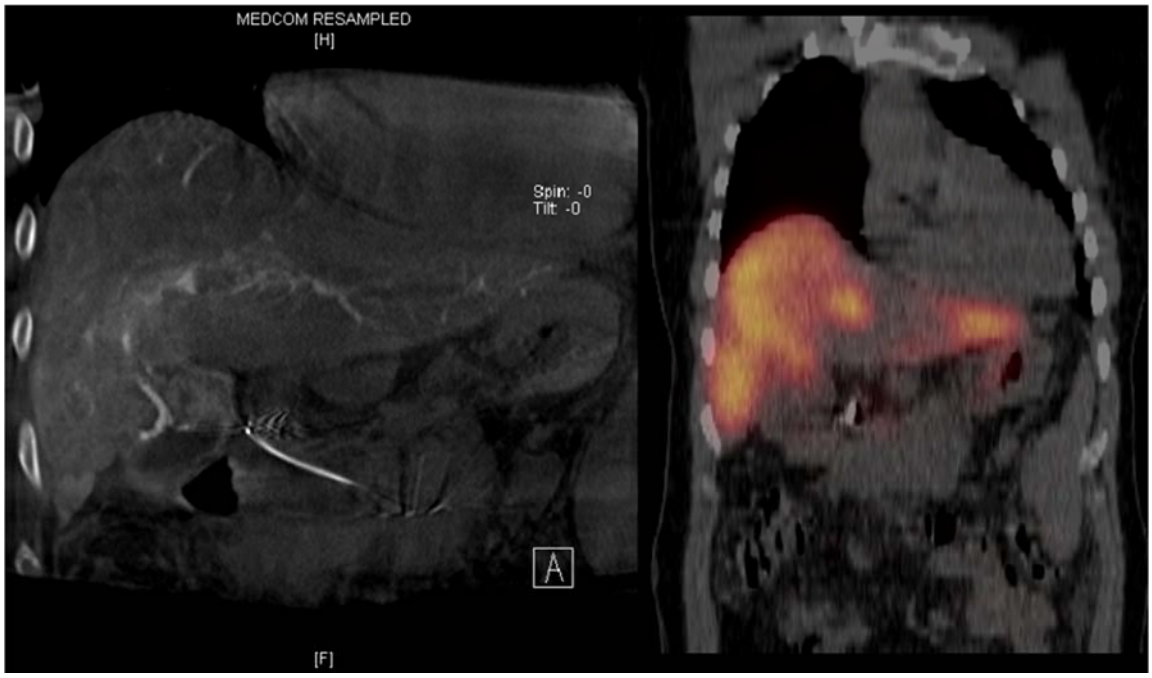

Figure 1: 56-year-old male with hepatitis C virus and unresectable hepatocellular carcinoma and portal vein tumor thrombosis administered 85.1 MBq of [^{99m}Tc]-MAA via a microcatheter placed in the right hepatic artery. The coronal SPECT/CT image and cone beam CTA demonstrates right to left hepatic shunt most likely as a result of portal vein tumor invasion.

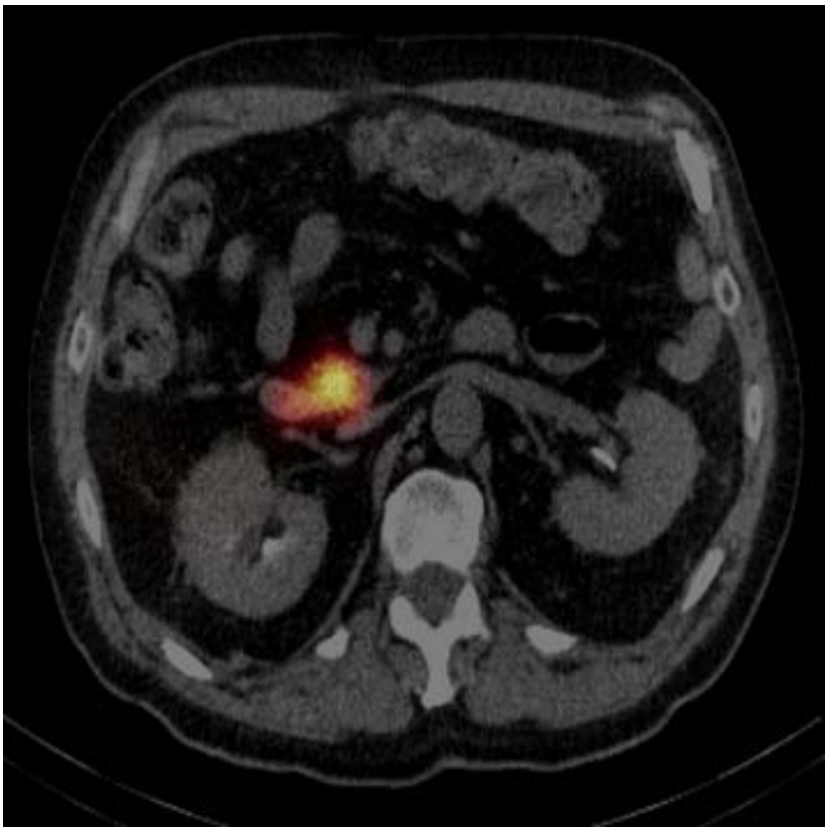

Figure 2: 63-year-old male with colon carcinoma metastatic to the liver was administered 85.1 MBq of ^{99m}Tc-MAA through a catheter placed in right hepatic artery proximal to the gastroduodenal artery; seventy-five minutes following administration, SPECT/CT study was performed. The transaxial slice from the reconstructed SPECT/CT image showed activity in the second portion of the duodenum.

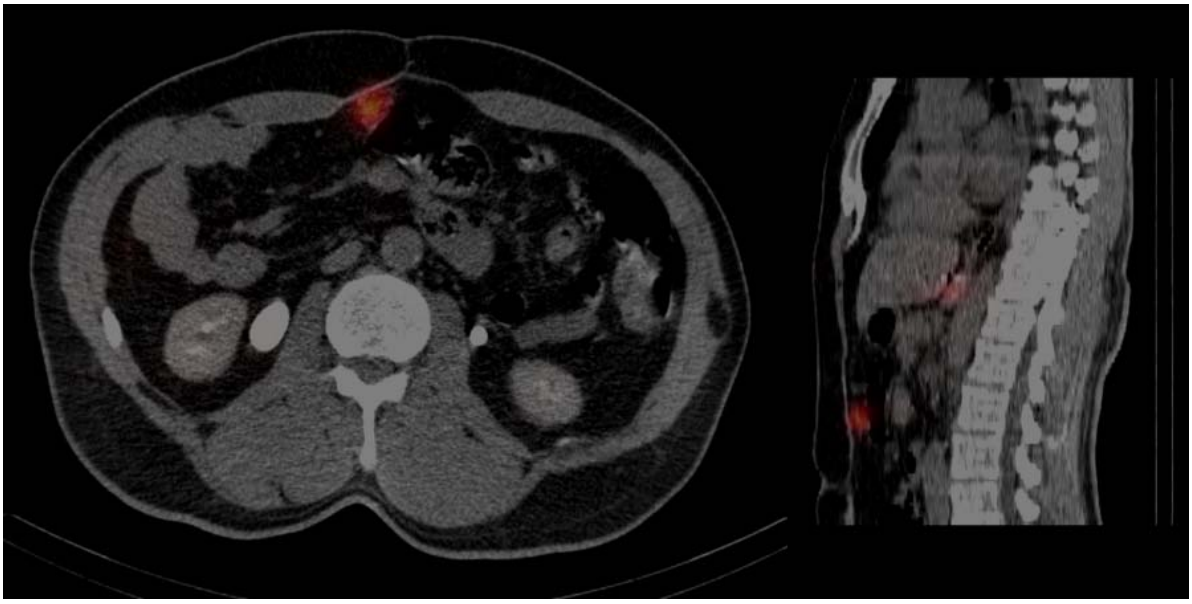

Figure 3: 58 year-old male with a history of metastatic neuroendocrine disease with hepatic involvement was administered 173.9 MBq of ^{99m}Tc-MAA through a microcatheter placed the middle hepatic artery. The transaxial and sagittal reconstructed SPECT/CT image shows ^{99m}Tc-MAA uptake within the anterior abdominal wall due to flow from the falciform artery, which originated from the middle hepatic artery.

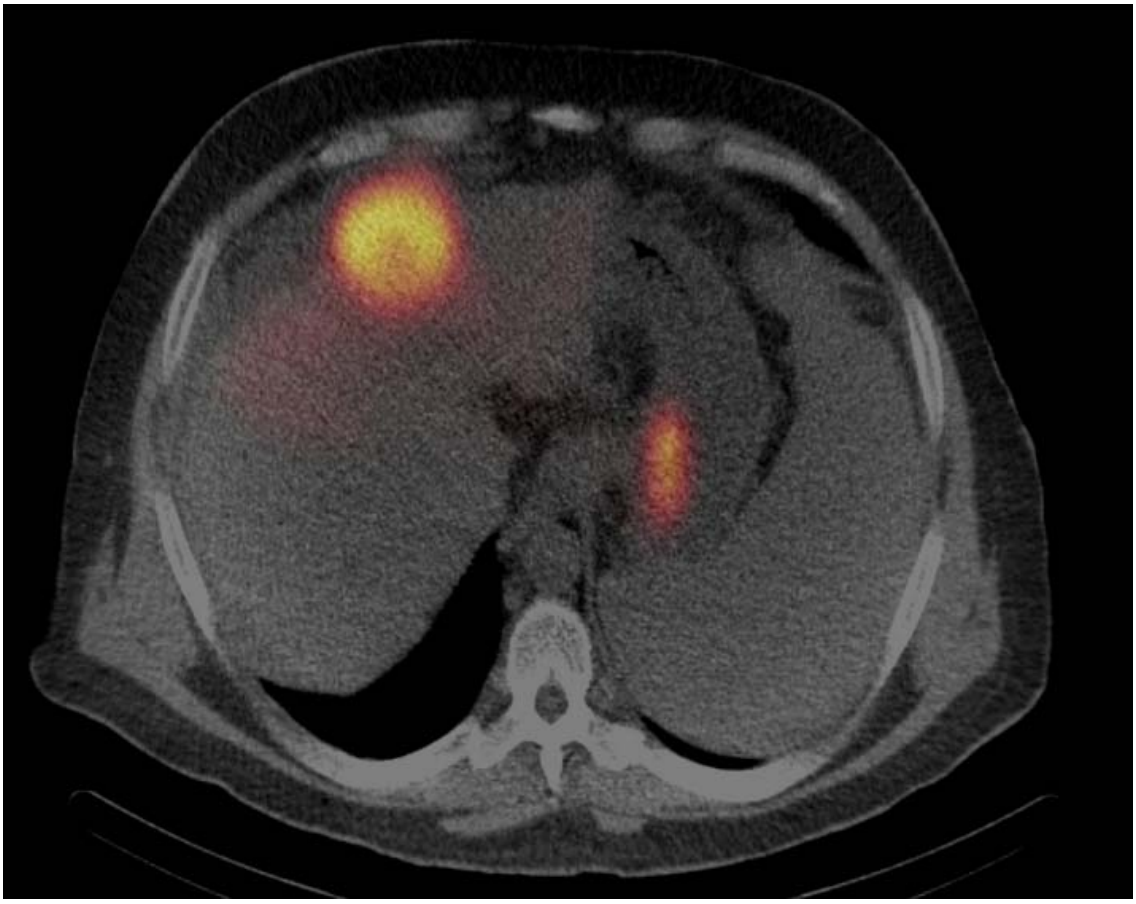

Figure 4: 76 year-old female with a history of hepatitis C infection and suspected hepatocellular carcinoma was administered 81.4 MBq of ^{99m}Tc-MAA through a catheter placed in middle hepatic artery and replaced left gastric artery. SPECT/CT images were subsequently obtained. Transaxial reconstructed SPECT/CT fused image of the medial left hepatic lobe, stomach, and spleen shows focal activity corresponding with the left lobe hepatoma and shows focal activity in the medial wall of the proximal stomach, indicating a significant abnormal shunting of the liver activity.

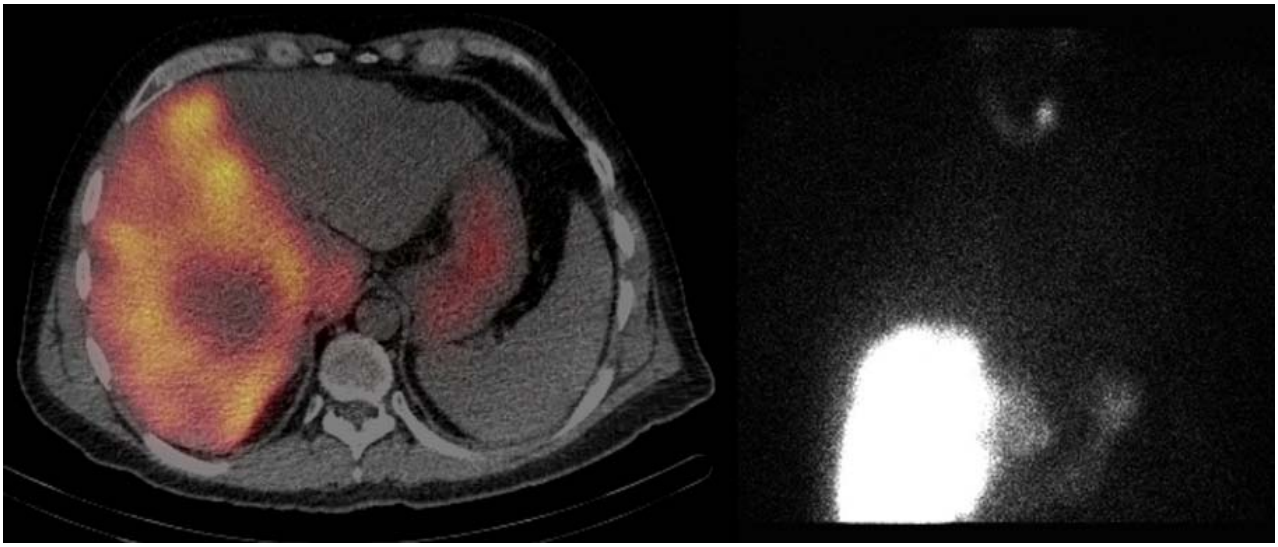

Figure 5: 45 year-old male with metastatic adenocarcinoma of the gastro-esophageal junction with hepatic involvement was administered 155.4 MBq of ^{99m}Tc-MAA through a catheter placed in right hepatic artery; following administration, a SPECT/CT study was performed. The transaxial slice from the reconstructed SPECT/CT image of the abdomen reveals that both the right hepatic and caudate lobes were perfused with an inhomogeneous distribution of activity corresponding to the patient's multifocal intra-hepatic lesions. In addition, free ^{99m}Tc pertechnetate can be observed in the lumen of the stomach. Incidentally noted is a focal area of increased uptake in the region of the left upper pole of the thyroid gland.

Table 1 Imaging results from this study and results from other published data

Categories	Subcategories	this study	Lenoir et al.(*13*) (2012)	Ahmadzadehfar et al. (*15*) (2010)	Hamami et al.(*16*) (2009)
Hepatic Distributions	Number of SPECT/CT	174	139	90	68
	NMI Intra-hepatic lobe distributions due to PVT (overall NMI)	62.5% (2.9%)	31% (7%)	NR	NR (4%)
	Angiogram Intra-hepatic lobe distributions due to PVT (overall and angiograms)	57.1% (2.3%)	NR	NR	NR
	Prior RFA or embolizations	13%	NR	NR	NR
	Distribution to the Caudate Lobe from right hepatic artery administrations	37% (19/51)	NR	NR	NR
Extra-Hepatic Distributions	Distributions from hepaticoenteric arterial communications as demonstrated on SPECT/CT	5%	9%	38%	24%
	Distributions from hepaticoenteric arterial communications as demonstrated on angiograms, DSA or CBCT with contrast	16%	NR	34%	28%
	Gallbladder Visualization	49%	12%	12%	9%
Normal Distribution Variants	Images indicating free pertechnetate or delabeled MAA	38%	22%	4%	NR
	Thyroid nodule, renal poles, reconstruction/metallic artifacts	3%	NR	NR	NR